

Ballistic to diffusive crossover in a weakly interacting Fermi gas

Jerome Lloyd

Department of Theoretical Physics, University of Geneva, 24 rue du Général-Dufour, 1211 Genève 4, Switzerland

Tibor Rakovszky

Department of Physics, Stanford University, Stanford, California 94305, USA

Frank Pollmann

*Department of Physics, T42, Technische Universität München, James-Frank-Straße 1, D-85748 Garching, Germany and Munich Center for Quantum Science and Technology (MCQST), Schellingstraße 4, D-80799 Munich, Germany*Curt von Keyserlingk *Department of Physics, King's College London, Strand WC2R 2LS, United Kingdom*

(Received 15 January 2024; revised 3 April 2024; accepted 5 April 2024; published 1 May 2024)

In the absence of disorder and interactions, fermions move coherently and their associated charge and energy exhibit ballistic spreading, even at finite energy density. In the presence of weak interactions and a finite energy density, fermion-fermion scattering leads to a crossover between early-time ballistic and late-time diffusive transport. The relevant crossover timescales and the transport coefficients are both functions of interaction strength, but the question of determining the precise functional dependence is likely impossible to answer exactly. In this work we develop a numerical method (fDAOE) which is powerful enough to provide an approximate answer to this question, and which is consistent with perturbative arguments in the limit of very weak interactions. Our algorithm, which adapts the existing dissipation-assisted operator evolution (DAOE) to fermions, is applicable to systems of interacting fermions at high temperatures. The algorithm approximates the exact dynamics by systematically discarding information from high n -point functions, and is tailored to capture noninteracting dynamics exactly. Applying our method to a microscopic model of interacting fermions, we numerically determine crossover timescales and diffusion constants for a wide range of interaction strengths. In the limit of weak interaction strength (Δ), we demonstrate that the crossover from ballistic to diffusive transport happens at a time $t_D \sim 1/\Delta^2$ and that the diffusion constant similarly scales as $D \sim 1/\Delta^2$. We confirm that these scalings are consistent with a perturbative Fermi's golden rule calculation, and we provide a heuristic operator-spreading picture for the crossover between ballistic and diffusive transport.

DOI: [10.1103/PhysRevB.109.205108](https://doi.org/10.1103/PhysRevB.109.205108)**I. INTRODUCTION**

Understanding the transport properties of materials is a central task in physics, providing an essential link between experiment and theory in condensed matter systems. The theoretical study of transport is also deeply connected to fundamental ideas in quantum chaos and many-body thermalization [1]. More recently, somewhat less obvious but nevertheless powerful connections have been drawn between transport and the study of entanglement growth, scrambling, and information spreading in many-body systems [2–5].

One unexpected result of the above connections has been to inspire new approaches to calculating transport properties numerically. Simulating quantum transport on classical

computers *exactly* is a difficult task because it requires simulating real-time dynamics to late times, and the memory required to store a time-evolved state tends to grow exponentially in time. On the other hand, in generic systems one expects that universal transport features emerge at late times which are captured by hydrodynamics, due to the system locally approaching thermal equilibrium [6]. Improved understanding of the generic behavior of operators under Heisenberg evolution has inspired new approximation schemes aimed at bridging these two levels of description in order to calculate transport coefficients from microscopic models with high accuracy [4,7–11].

So far these methods have focused on systems of lattice spins, such as Ising or Heisenberg spin chains. However, given that the archetypal condensed matter system is, arguably, the interacting electron gas, developing numerical methods for the transport properties of fermionic systems is equally important. Such methods could be of use in taming outstanding experimental mysteries relating to the transport properties of strongly correlated electron systems (e.g., [12]), but also

Published by the American Physical Society under the terms of the Creative Commons Attribution 4.0 International license. Further distribution of this work must maintain attribution to the author(s) and the published article's title, journal citation, and DOI.

help in quantitatively reconciling effective theories with experiment and predicting trends in transport properties with changes in experimental conditions. They would also be of use in guiding and benchmarking transport experiments in analog quantum simulators [13–16].

In this paper we generalize one such method to fermions, and use it to probe the physics of an interacting fermion system. The method, called “dissipation-assisted operator evolution” (DAOE), evolves observables in real time, using the Heisenberg picture, and applies a truncation scheme based on the size of their spatial support. The intuition behind this approximation, substantiated by numerical and analytical calculations in Refs. [7,11], is that the contribution to transport coefficients from highly nonlocal observables decreases sharply (indeed, exponentially [11]) with their support.

The original formulation of DAOE [7] does not directly apply as it is formulated in terms of spin rather than fermionic variables. However, we expect that similar approximations should apply to systems of interacting fermions. While, at least in one dimension (which is where DAOE currently applies), the two can be related by the Jordan-Wigner transformation, the relevant notion of “operator support” is very different in the two cases, due to the nonlocality of the transformation; indeed, 2-body fermionic operators map onto long nonlocal strings in the spin language. As a consequence, applying DAOE in the naive way fails to capture the limit of weakly interacting fermion systems, including the exactly solvable free-fermionic case, as we demonstrate explicitly below. Instead, we develop a modified approximation scheme, named fermionic DAOE (fDAOE), which keeps few-body fermionic observables exactly, while truncating higher order ones in a tunable way (tuned by the strength of an artificial dissipation). It is therefore exact for free fermions and provides a good starting point to incorporate the effects of fermion-fermion scattering.

A particularly interesting test case for our fermionic method is in the limit of weak, but nonvanishing interactions. In the fully noninteracting limit, and in the absence of disorder, electrons propagate *ballistically* and coherently (i.e., the fermion propagator exhibits a characteristic interference pattern due to quantum mechanical effects). However, when many electrons interact, their collisions tend to wash out interference effects at long times, typically leading to a *diffusive* charge transport at finite temperatures [17]. One therefore expects a ballistic to diffusive crossover which happens at parametrically late times when interactions are weak (correspondingly, the resulting diffusion constant is also parametrically large in this regime). These characteristically large timescales make it challenging to capture the behavior of these systems accurately. Novel numerical approaches are therefore needed. The fact that fDAOE becomes exact when interactions are turned off makes it a promising candidate to tackle this challenge.

In the weakly interacting regime, it is possible to use perturbation theory [in the guise of Fermi’s golden rule (FGR), as we will discuss in Sec. V] to argue that diffusion constants and scattering timescales scale as $O(1/\Delta^2)$ where Δ is the interaction strength. However, such arguments are ultimately uncontrolled, as witnessed by the fact that weakly interacting integrable models have interactions but do not exhibit

diffusion at small Δ . So, while FGR can be used to estimate the timescales when a free-fermion approximation breaks down,¹ it does not give access to transport features at asymptotically late times, which are inherently nonperturbative. This lack of analytical control makes necessary the development of the numerical tools in this work.

In this work, we consider a nonintegrable one-dimensional model of fermions with a tunable interaction strength Δ . We demonstrate the power of fermionic DAOE by showing that it can obtain well-converged results for a whole range of interactions, from free to strongly coupled fermions, unlike either brute-force matrix product state methods [18,19], which fail to capture the interacting case due to the rapid growth of entanglement, or spin-based DAOE, which fails already at the noninteracting level. By following the dynamics to late times, we find the expected crossover to diffusive transport, and fit its timescale to be $t_D \propto 1/\Delta^2$. We also fit the diffusion constant itself and find evidence of similar scaling with Δ . Finally we outline a Fermi’s golden rule perturbative calculation, which supports this scaling, and provide a picture for the ballistic to diffusive crossover in the language of operator spreading.

II. DAOE METHOD

DAOE [7] is an algorithm for calculating dynamical correlation functions in interacting quantum systems. It can be used to extract transport coefficients via linear response theory. In this paper we focus on calculation of the diffusion constants, which measures how initial perturbations in globally conserved densities (charge, spin, etc.) spread throughout the system. We first describe how this is done in the existing version of DAOE (which we will refer to as “spin DAOE”), before describing its modification in the fermionic context.

A. Spin DAOE

Denote by q_x the local density at site x of the globally conserved quantity Q . We consider one-dimensional systems of length L , and take $x = 0$ to label the site in the center of the chain. Without loss of generality assume that $\langle q_x \rangle = 0$ at equilibrium, and is normalized such that $\sum_x \langle q_0 q_x \rangle = 1$, where $\langle A \rangle = \text{tr}(A\rho)$ and ρ is the equilibrium density matrix. We work at infinite temperature throughout, so that $\langle A \rangle = \text{tr}(A)/\mathcal{N}$, \mathcal{N} being the Hilbert space dimension. The associated diffusion constant is then given by $D \equiv \lim_{t \rightarrow \infty} D(t)$ where

$$D(t) = \lim_{L \rightarrow \infty} \partial_t \sum_x \frac{x^2}{2} \langle q_x | \mathcal{U}(t, 0) | q_0 \rangle. \quad (1)$$

Here the superoperator \mathcal{U} evolves operators in the Heisenberg picture,

$$\langle A | \mathcal{U}(t_2, t_1) \equiv \langle U^\dagger(t_2, t_1) A U(t_2, t_1) |, \quad (2)$$

and we introduced an inner product between operators $\langle A | B \rangle \equiv \langle A^\dagger B \rangle$.

¹Even this estimate is quite delicate, and difficult to make rigorous, at least in one dimension, as we discuss in Sec. V.

The difficulty of evaluating Eq. (1) lies in the fact that in generic systems, the memory required to accurately store the time-evolved operator, for example in a matrix product operator representation, grows exponentially in time, due to the linear Lieb-Robinson light cone, which makes an exact evaluation of the necessary correlation functions prohibitively expensive [20,21]. In DAOE, this is circumvented by truncating the operator content, on the premise that much of the information stored in nonlocal operators is irrelevant for computing the overlaps $\langle q_x(t)q_0 \rangle$ between local observables, as elaborated below.

The algorithm is implemented as follows. In Eq. (1), we replace the unitary evolution $\mathcal{U}(t, 0)$ with the periodically dissipated evolution $\tilde{\mathcal{U}}(t, 0) \equiv \prod_{j=0}^{t/T-1} [\mathcal{U}(t_{j+1}, t_j) \mathcal{G}_{\ell_*, \gamma}]$. The dissipation superoperator $\mathcal{G}_{\ell_*, \gamma}$ is applied with a period T (with $t_j = jT$ and t/T assumed to be integer) and designed to suppress operators larger than some cutoff length ℓ_* . In a spin-1/2 system, $\mathcal{G}_{\ell_*, \gamma}$ can be defined by its action on *Pauli strings* $|\sigma^\mu\rangle$. These are tensor products of matrices $I, \sigma^{x,y,z}$ on the different sites of the chain, which form a basis (of size 4^L) for the space of all operators acting on the spin chain. The dissipator then takes the form

$$\mathcal{G}_{\ell_*, \gamma} |\sigma^\mu\rangle = e^{-\gamma \max(0, \ell(\mu) - \ell_*)} |\sigma^\mu\rangle, \quad (3)$$

where $\ell(\mu)$ —the “length” of operator σ^μ (also known as the *Pauli weight*)—is the number of nonidentity matrices in the string σ^μ . Using this nomenclature, note that the operator $\sigma_1^z \sigma_{27}^x$ has length $\ell = 2$, even though it is spread over a large spatial region (of diameter 27). This is the form of DAOE that appeared in Refs. [7,11].

How does this artificial dissipation help in evaluating Eq. (1)? As was shown in Ref. [7], the dissipation cuts off the growth of the effective entanglement of the state $|q_x(t)\rangle$ (the operator space entanglement entropy, or OSEE [20,22]). This means that $|q_x(t)\rangle$ can be efficiently represented as a *matrix product state* (MPS), which allows one to use standard tensor network techniques, such as time-evolving block decimation (TEBD) [23], to perform the time evolution efficiently; the errors made by truncating to a finite bond dimension will depend only on the amount of dissipation used, and they will remain bounded at all times, unlike the case for purely unitary dynamics where entanglement grows without bound [20,21]. The operator $\mathcal{G}_{\ell_*, \gamma}$ defined by Eq. (3), itself has a compact representation as a matrix product operator (MPO) representation with bond dimension $\ell_* + 1$, which makes its application efficient.

While the introduction of the dissipation renders the numerical calculation of correlations feasible, it will also introduce errors; i.e., the diffusion constant of the dissipative dynamics, $D_{\ell_*, \gamma}$, will be different from the true physical diffusion constant D . The insight behind DAOE is that the error made in this approximation should be well controlled when the dissipation is sufficiently weak, allowing for an accurate estimation of the true diffusion constant. The reason behind this is that once an operator becomes highly nonlocal, its contribution to correlation functions of local observables becomes suppressed, due to a combination of entropic and interference effects [11]. More quantitatively, in Ref. [11] some of us conjectured, based on numerical evidence and

analytical arguments, that this error is suppressed exponentially, as $|D - D_{\ell_*, \gamma}| \leq ae^{-b\ell_*}$ at large ℓ_* . More practically, one calculates $D_{\ell_*, \gamma}$ for decreasing values of γ until the limit of the available numerical resources is reached,² and then uses the results to perform an extrapolation back to the nondissipative case: $D = \lim_{\gamma \rightarrow 0} D_{\ell_*, \gamma}$. This limit should be independent of the choice of ℓ_* , which provides a further consistency check on the results [7].

B. Modified DAOE for fermions (fDAOE)

The spin DAOE we just described is formulated for systems of lattice spins, appropriate for simulating transport in quantum magnets [24–26]. However, one often wants to obtain information about transport in systems of fermions, where we can ask about the transport of electric charge. The physical intuition behind DAOE is general enough that it should apply to this case as well, assuming that one is at a finite temperature where electron scattering should render transport incoherent. Thus, it is natural to formulate a fermionic version of DAOE, which is what we obtain here, working still in one dimension.

We consider Hamiltonian dynamics which conserve the total fermion charge, $[H, \sum_x n_x] = 0$, with $n_x = f_x^\dagger f_x$ the local charge density and f_x^\dagger, f_x the standard spinless fermion creation-annihilation operators. To calculate charge transport, we need to evaluate connected correlations of the form $\langle n_x(t) n_y(t') \rangle^c$. In one-dimensional systems, one possibility is to make use of the Jordan-Wigner transformation to rewrite fermionic operators in terms of spins, and then apply spin DAOE in this new formulation. However, this is complicated by the fact that the transformation between the two variables is nonlocal; thus, the notion of Pauli weight that we used to truncate nonlocal observables in spin DAOE is not the appropriate measure of locality.

The problems with this naive approach can be observed already at the level of noninteracting fermions. In this case the time evolution of a single-fermion operator f_x^\dagger maps into a coherent superposition of 1-body operators

$$f_x^\dagger \rightarrow \sum_y K_{y,x}(t) f_y^\dagger, \quad (4)$$

where K is the noninteracting lattice Feynman propagator. The time-evolved charge density takes the form $n_x(t) = \sum_{y,y'} K_{xy}(t) K_{xy'}^*(t) f_y^\dagger f_{y'}$. For translationally invariant Hamiltonians on the lattice, the free Feynman propagator $K_{xy}(t)$ is generically nonvanishing only within a light cone $|y - x| < vt$, where it has amplitude roughly $1/\sqrt{t}$. The result of this is that density spreads ballistically; i.e., $\langle n_x(t) n_y(t') \rangle^c$ is nonvanishing only when $|x - y| < vt$ (and has typical size $\sim 1/t$ within the light cone). By Eq. (1), this implies that the time-dependent diffusion constant grows linearly as $D(t) \sim t$.

²The weaker the dissipation, the larger the maximum of the OSEE reached during the dynamics, implying that one will need increasingly large bond dimensions to get accurate results.

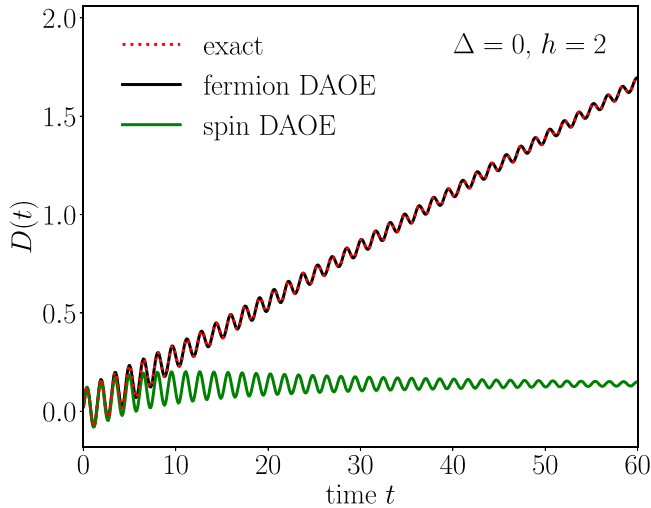


FIG. 1. For the noninteracting case $\Delta = 0$, $h = 2$ of the model defined in (7), we show $D(t)$ vs t as determined by different methods. The red dotted line is the exact result calculated from the free-fermion propagator $K(t)$, with the ballistic scaling $D(t) \sim t$. Fermion DAOE agrees with the exact result provided $\ell_* \geq 2$. Spin DAOE, however, gives incorrect diffusive behavior past short times even in the $\Delta = 0$ case, due to heavily truncated Jordan-Wigner strings. The DAOE parameters were taken as $\gamma = 0.1$, $\ell_* = 2$, $\delta t = 0.5$ in both cases (the fDAOE results are independent of the parameters in the noninteracting case, provided $\ell_* \geq 2$).

To apply spin DAOE to this problem, we can make use of the Jordan-Wigner transformation

$$f_x^\dagger = \left[\prod_{s < x} \sigma_s^z \right] \sigma_x^+ . \quad (5)$$

This turns the operators $f_y^\dagger f_{y'}$, appearing in the calculation of $n_x(t)$, into strings of spin variables stretching from y to y' . As we say, the typical terms contributing to $n_x(t)$ have $|y - y'| = O(t)$, and hence $\ell = O(t)$. Therefore at sufficiently late times compared to ℓ_* , $n_x(t)$ contains long strings of spin operators which will be subject to the DAOE dissipation under the existing scheme. This suggests that the existing DAOE approach, while effective in capturing the diffusive part of the dynamics, will fail to correctly account for the ballistic spread of charge in the limit of weak interactions.

This expectation is confirmed in Fig. 1 where we show the measured time-dependent diffusion constant of the charge density for free-fermion dynamics [$h = 2$, $\Delta = 0$ in the model defined in Eq. (7) below], with DAOE truncating according to Pauli weight of the Jordan-Wigner transformed operators (green line). The results show a very rapid onset of diffusion, whereas the true behavior, as calculated from the noninteracting propagator $K(t)$, is ballistic (red dotted line).

As previously alluded to, the issue lies in the use of the Pauli weight for truncating fermionic systems. A natural generalization of DAOE is instead to truncate operators based on their fermion operator weight (*Fermi weight*). To make this notion precise, we introduce the Fermi strings $|\sigma^\mu\rangle$, in analogy to the Pauli strings $|\sigma^\mu\rangle$. A complete on-site basis of operators is given by the four operators $\sigma^{1,2,3,4} = I, f^\dagger, f, [f^\dagger, f]$, which have Fermi weights 0,1,1,2 respectively. In the

following we use the variable z as a shorthand for $[f^\dagger, f] = 2f^\dagger f - I$. The Fermi strings $\sigma^\mu \equiv \otimes_r \sigma_r^\mu$ are tensor products of the local basis operators on L sites, and we define the Fermi weight of σ^μ as the sum of its on-site weights. For example, the string $f_2^\dagger f_6^\dagger f_6$ has Fermi weight $\ell = 3$. Now, quadratic operators such as $f_y^\dagger f_{y'}(t)$ evolved under noninteracting dynamics have weight $\ell = 2$ for all times, even if y, y' are well separated. The only change needed in the definition of the DAOE dissipator [Eq. (3)] is replacing the Pauli weight with the Fermi weight.

Provided we choose cutoff $\ell_* \geq 2$, dissipation will not interfere with the early-time ballistic behavior of correlation functions. In the case of $\Delta = 0$, comparing $D(t)$ calculated using fermion DAOE in Fig. 1 (black line), we observe perfect agreement with the exact result. We refer to the Fermi weight truncated DAOE as fDAOE. In Appendix A we provide further comparison between the spin and fermion algorithms for different interaction strength Δ , showing that spin DAOE remains inaccurate in the weakly interacting regime $\Delta \ll 1$, while the two methods begin to agree around $\Delta = O(1)$.

In order for fDAOE to remain efficient, we still need to be able to write the dissipator in a compact MPO format. This turns out to be possible, following the method of [27], as we now describe.

We first design a “finite-state automata” \mathcal{W} that takes as its input a Fermi string $|\sigma^\mu\rangle$ (equivalently a Pauli string $|\sigma^\mu\rangle$, as the two can be mapped via the Jordan-Wigner transform), calculates the corresponding Fermi weight $\ell(\mu)$, and outputs a weighted copy $e^{-\gamma \max(0, \ell(\mu) - \ell_*)} |\sigma^\mu\rangle$. The automata’s calculation can be visualized as a machine that moves along the input string $|\sigma^\mu\rangle$, reading the operator at each position x from left to right, and updating its internal state based on this new information and its current state, finally outputting the desired weighting. Having constructed our finite-state automata, we finally have to convert it into an MPO. This can be done with virtual bond dimension $\ell_* + 1$, as in the spin DAOE case. We explain the case $\ell_* = 4$ in detail, with the extension to other ℓ_* straightforward. We restrict ourselves to the case where all Fermi strings have even parity, which provides no loss of generality when the system obeys charge conservation.

The fDAOE automata for $\ell_* = 4$ is drawn on the left of Fig. 2. We consider the automata’s action on the example fermion string given in the top row of the table on the right of Fig. 2. The fermion string is mapped to the Pauli string in the second row via the Jordan-Wigner transform (this step is required as numerically our MPO must operate on Pauli strings). The machine starts at the first site of the string in an initial state $s = 1^+$. It then reads the operator at the current site. Following the map on the left of Fig. 2, there are then three possibilities: if the operator is I , the automata remains in state 1^+ ; if the operator is σ^z , the automata updates its state to $s = 2^+$; otherwise, the operator is either σ^+ or σ^- , and the automata sets its new state as $s = 1^-$ (the \pm index can be read as a parity label, in a sense made clear below). It then moves to the second site of the chain, and repeats the above steps, following the new directions based on its current state. The state label allows us to keep track of the Fermi weight and whether ℓ_* has been exceeded: for every red dashed line the automata follows (e.g., from state 3^+ to 2^-), the input string is multiplied by a damping factor $e^{-2\gamma}$. The resulting automata

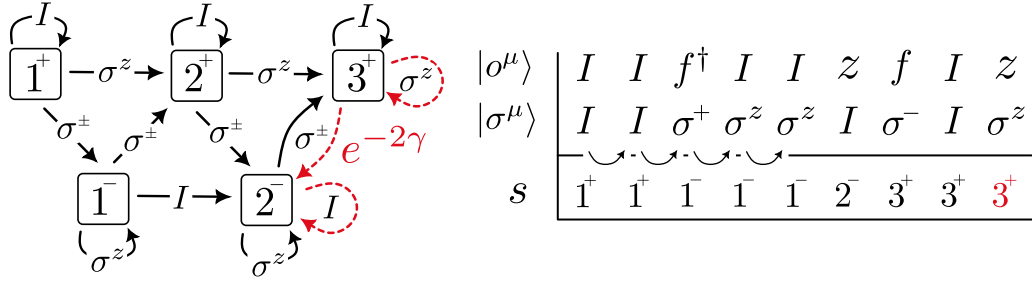


FIG. 2. Left: A 5-state finite automata for fDAOE with $\ell_* = 4$. See text for details. Right: Example fermion string $|\sigma^\mu\rangle$, corresponding Jordan-Wigner mapped Pauli string $|\sigma^\mu\rangle$, and automata trajectory s .

“trajectory” for the example string above is given in the third row of the table in Fig. 2: the string $|\sigma^\mu\rangle$ has Fermi weight $\ell = 6$ and is correctly weighted by the automata with a factor $e^{-2\gamma}$. In general, for a given (even) ℓ^* , the automata has states i^+ for $1 \leq i \leq \ell^*/2 + 1$, and states i^- for $1 \leq i \leq \ell^*/2$.

The key point is that to correctly account for the nonlocality of the Jordan-Wigner transform, the automata must keep track of the fermion parity, i.e., the number of fermions to the left of its current position. A pair of spatially separated fermions f^\dagger, f (connected by a string of identity operators) maps to a pair of σ^\pm operators connected by a string of σ^z operators in the Pauli basis. In order for these σ^z to not count toward the Fermi weight, the automata must switch to the negative-parity branch $1^-, 2^-, \dots$ where the roles of σ^z and I are exchanged. This parity switching is the reason why fDAOE correctly captures the noninteracting fermion dynamics, while spin DAOE truncates quadratic strings.

Given the finite-state machine, it is then simple to construct the corresponding MPO. We refer to [27] for details and simply state the result for $\ell_* = 4$. The local MPO tensor $W_{ab}^{ii'}$ acts diagonally on the physical leg index $i = I, +, -, Z$, $W_{ab}^{ii'} \propto \delta_{ii'}$, and as a matrix on the virtual leg index $a = 0, \dots, \ell_*$. Owing to the even-parity constraint, ℓ_* must be even. Explicitly the matrices are given by

$$\begin{aligned}
 W^{II} &= \left(\begin{array}{ccc|cc} 1 & 0 & 0 & 0 & 1 \\ 0 & 1 & 0 & 0 & \kappa \\ 0 & 0 & 1 & 0 & 0 \end{array} \right), \\
 W^{ZZ} &= \left(\begin{array}{ccc|cc} 0 & 1 & 0 & 1 & 0 \\ 0 & 0 & 1 & 0 & 1 \\ 0 & 0 & \kappa & 0 & 0 \end{array} \right), \\
 W^{\pm\pm} &= \left(\begin{array}{ccc|cc} & & & 1 & 0 \\ & & & 0 & 1 \\ & & & 0 & \kappa \\ 0 & 1 & 0 & 0 & 0 \\ 0 & 0 & 1 & 0 & 0 \end{array} \right). \quad (6)
 \end{aligned}$$

Here we split the matrices into parity blocks $++$, $+-$, $-+$, $--$: the even-parity (+) indices run from 0 to $\ell_*/2$, and the odd-parity indices (−) from $\ell_*/2 + 1$ to ℓ_* . For example, the W^{II} matrix right-multiplies the machine state $1^- = (0, 0, 0, 1, 0)$ and returns the state $2^- = (0, 0, 0, 0, 1)$. The

damping factor $\kappa = e^{-2\gamma}$ is applied on transitions corresponding to the red dashed lines in Fig. 2. The MPO is contracted on the left boundary with the vector $v_L = (1, 0, \dots, 0)$ —representing the initial state 1^+ —and with $v_R = (1, 1, \dots, 1)$ on the right.

The fDAOE dissipator can hence be applied in an efficient way to operators represented as matrix product states $|q(t)\rangle$. This is the first main result of this work.

While above we assumed spinless fermions in 1D for simplicity, the algorithm can easily be extended to more complicated setups. First, we may treat the case of spinful fermions: this can be done by doubling the number of lattice sites and treating the spin label as an additional sublattice label when applying the automata. Hence, for example, the string $f_{1,\uparrow} f_{1,\downarrow} f_{3,\uparrow}^\dagger$ becomes $f_1 f_2 f_5^\dagger$ and the fDAOE automata is applied just as in the spinless case, giving the correct weighting $\ell = 3$. The extension to higher dimensions also follows straightforwardly once the Jordan-Wigner string ordering has been defined. For example, in 2D we can order the sites along a 1D “snake” winding over the lattice, and apply the fDAOE MPO in this ordering. The dimension of the MPO tensors remains $\ell_* + 1$ and hence the fDAOE step is efficient. The more serious problem arises from the unitary time evolution step, since local couplings in 2D will be mapped to nonlocal couplings under the Jordan-Wigner map, a standard problem in higher-dimensional simulations. In the cases where the time evolution step can be implemented efficiently (such as for quasi-1D cylinders of small width), we expect the fDAOE algorithm to remain efficient.

III. MODEL

For the rest of this work we focus on the physics of hopping spinless fermions with a staggered chemical potential:

$$\begin{aligned}
 H &= - \underbrace{\sum_x \left(\frac{J}{2} (f_{x+1}^\dagger f_x + \text{H.c.}) + h(-1)^x (1 - 2n_x) \right)}_{H_0} \\
 &+ \Delta \underbrace{\sum_x (1 - 2n_x)(1 - 2n_{x+1})}_{\Delta \times V}. \quad (7)
 \end{aligned}$$

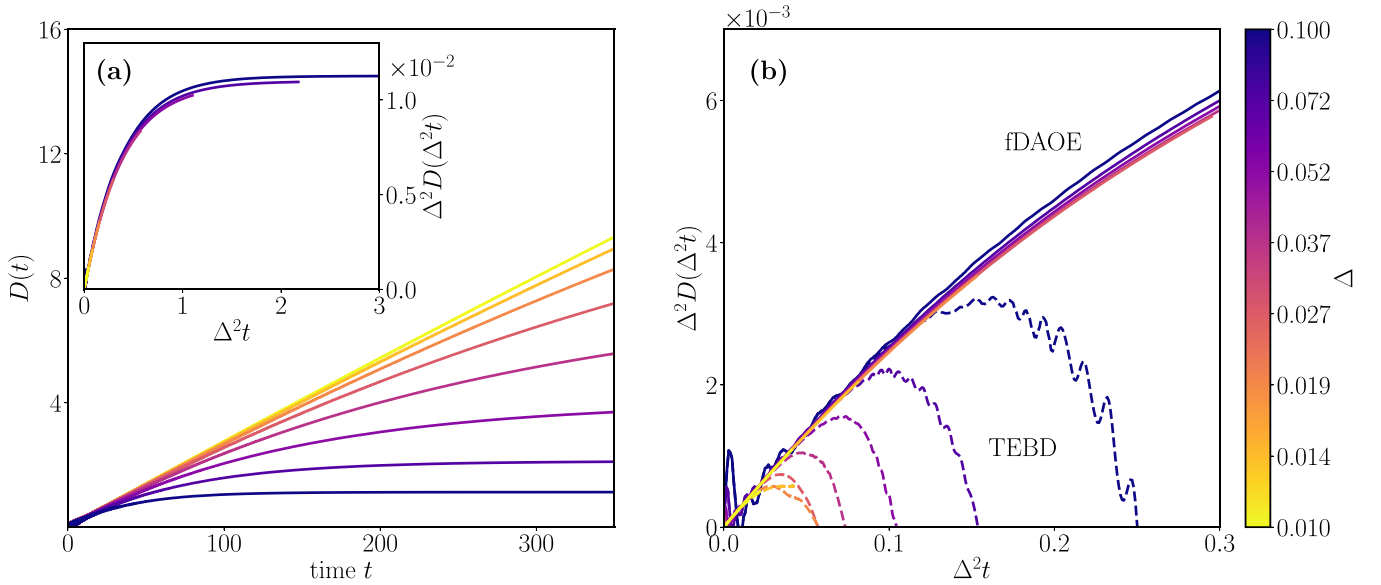


FIG. 3. (a) Growth of time-dependent diffusion constant $D(t)$, for eight different interaction strengths Δ , as marked on the right-hand color bar (note the log scale). For increasing Δ , the timescale at which transport becomes diffusive decreases, with a late-time diffusive plateau reached for the strongest interactions around $t = 200$ – 300 . Inset: Scaling collapse of rescaled diffusion constant $\Delta^2 D(\Delta^2 t)$. The diffusion constant grows linearly at early times $\Delta^2 t \ll 1$, before a crossover to diffusive transport occurs at late times $\Delta^2 t \gg 1$, where the curve saturates. (b) Zoom on $\Delta^2 D(\Delta^2 t)$ for short times, with TEBD simulations (dashed lines) overlaid. For all Δ , TEBD fails to reach the crossover timescale $\Delta^2 t \sim 1$, due to an accumulation of truncation errors arising from unchecked entanglement growth. For both figures, we fix DAOE parameters $\gamma = 0.1$, $\ell_* = 2$ and maximum bond dimension $\chi = 96$ for fDAOE, $\chi = 128$ for TEBD.

By the Jordan-Wigner mapping, the Hamiltonian can also be written as the staggered-field XXZ Hamiltonian,

$$H = \sum_x \left(\frac{J}{2} (\sigma_x^+ \sigma_{x+1}^- + \text{H.c.}) + h (-1)^x \sigma_x^z \right) + \Delta \sum_x \sigma_x^z \sigma_{x+1}^z. \quad (8)$$

This model (first introduced in [28]) is nonintegrable if all three couplings J, h, Δ are nonzero. In particular, switching on the staggered field h breaks the integrability of the XXZ model. We will focus on the regime where $\Delta \ll J, h$. At $\Delta = 0$ the fermions are noninteracting, and exhibit the ballistic transport we observed in Fig. 1. Turning on Δ turns this into a problem of interacting fermions. We will be interested in how charge transport is affected by these interactions.

IV. NUMERICAL RESULTS

We now use fDAOE to study the ballistic to diffusive crossover in the model of interacting fermions in Eq. (7). We fix the model parameters $J = 1$ and $h = 2$, and vary the interaction strength Δ . As explained above, the model is no longer integrable when $\Delta \neq 0$, and diffusive transport is expected at late times.

We use fDAOE to simulate the evolution of the infinite-temperature density-density correlator $C(x, t) = \langle q_x(t) | q_0(0) \rangle$, with $q_x = \sigma_x^z$, and $x = 0$ denoting the central site. This spin correlator is related to the connected fermion charge-charge correlator by $C(x, t) = 4 \langle n_x(t) n_0(0) \rangle^c$. We then calculate the time-dependent diffusion constant $D(t)$ using Eq. (1). All of our simulations are done using the TeNPy package [29] which allows us to make use of the

system's charge conservation property for more efficient simulations. Throughout the rest of the paper we fix the (2nd order) TEBD time step $\delta t = 0.1$, DAOE truncation period $T = 0.5$, and chain length $L = 300$, which is large enough that boundary effects are not observable on the times we study (the maximum times we reach are around $t = 350$, using around 100 h of wall time).

In Fig. 3(a) we plot the growth of the time-dependent diffusion constant $D(t)$ against time t , for different Δ . We fix DAOE parameters as $\gamma = 0.1$, $\ell_* = 2$ and show results for eight logarithmically spaced Δ in the interval $(0.01, 0.1)$. The data shown are for bond dimension $\chi = 96$; we provide additional convergence data in Appendix B. The crossover behavior is evident for sufficiently large Δ , with an initial ballistic growth $D(t) \propto t$, followed by a late-time plateau to diffusion $D(t) \sim D$ (the value of which generally depends on Δ as well as the DAOE parameters; see below). The results for the smallest Δ values remain approximately ballistic up to the largest times simulated.

To determine how $D(t)$ depends on Δ , we perform a rescaling of the time $t \rightarrow \Delta^2 t$ and the diffusion constant $D(t) \rightarrow \Delta^2 D(\Delta^2 t)$. In the inset to Fig. 3(a), we plot the rescaled dependence. We observe a clean scaling collapse of the data, consistent with the approximate scaling $D \propto \Delta^{-2}$ and a ballistic to diffusive crossover time (when the coherent transport of charge crosses over to diffusive transport) $t_D \sim \Delta^{-2}$. This scaling is consistent with a perturbative argument following Fermi's golden rule which we outline in Sec. V.

We next attempt to extrapolate the infinite-time diffusion constant $D \equiv \lim_{t \rightarrow \infty} D(t)$, as a further check on the scaling result. We consider the five largest Δ values in the same dataset (for smaller Δ , the simulations do not reach far enough

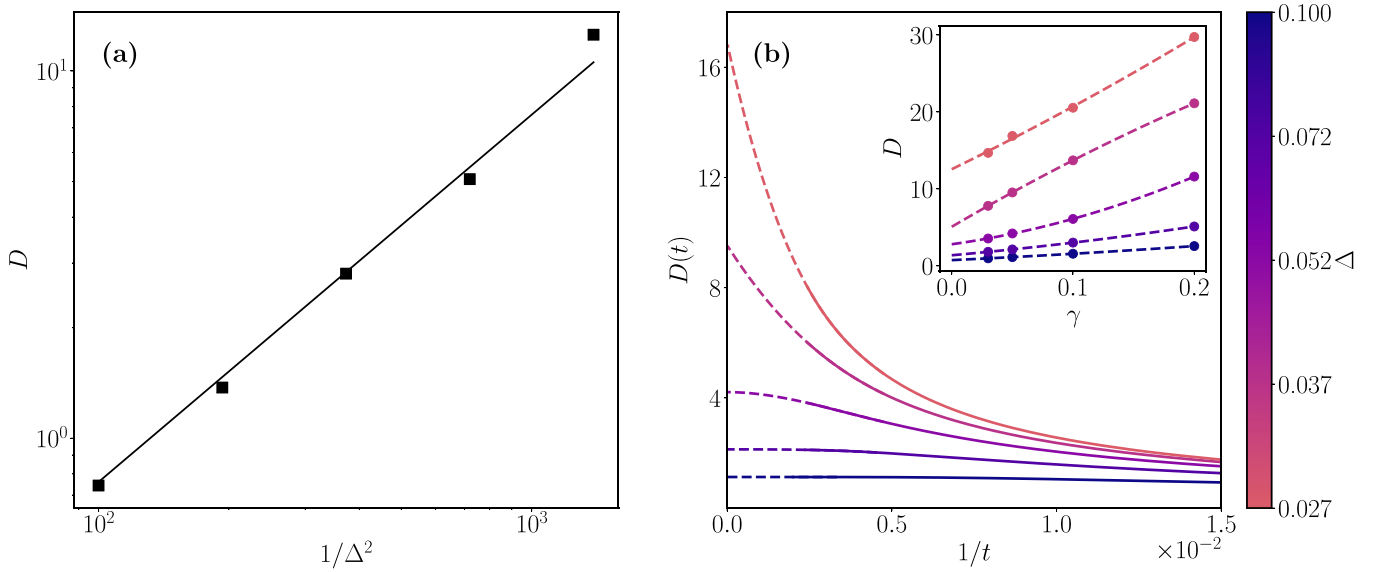


FIG. 4. (a) Late-time diffusion constant $D \equiv \lim_{t \rightarrow \infty} D(t)$ as a function of interaction strength Δ (we show only the largest five Δ , as the smaller Δ data are not sufficiently diffusive at the maximum run-time to obtain accurate extrapolation). The data are extrapolated in $\gamma \rightarrow 0$. The fit is the function $D = d\Delta^{-2}$, with the fit parameter $d = 0.01$. (b) Extrapolation of D : We fit $D(t)$ to a cubic polynomial in the inverse time variable $1/t$ at late times, with D as the y -axis intercept. Solid lines are data and dashed lines are the fit. Data shown are for $\gamma = 0.05$. Inset: Extrapolation in $\gamma \rightarrow 0$: For each data point the diffusion constant is obtained by the previous method, then we fit the data to a quadratic polynomial in powers of γ (dashed lines).

into the diffusive regime to achieve a reliable estimate), and fit the late-time data to a cubic polynomial in the inverse time variable, i.e., $D(t) \sim D - a/t + b/t^2 + c/t^3$. The resulting diffusion constants D are then extrapolated in $\gamma \rightarrow 0$ for the four values $\gamma \in (0.03, 0.05, 0.1, 0.2)$, for each Δ . We use a quadratic fit for the extrapolation in γ . The result is shown in Fig. 4(a), with the scaling $D \sim \Delta^{-2}$: the black line is the fit $D = 0.01\Delta^{-2}$. In Fig. 4(b) we show additional details of the extrapolation process, with the $1/t$ extrapolation for $\gamma = 0.05$ shown in the main figure and the subsequent γ extrapolation in the inset.

Our results for the diffusion constant $D \sim \Delta^{-2}$ and crossover timescale $t_c \sim \Delta^{-2}$ provide a convincing picture of how diffusion arises from weak fermion-fermion scattering at late times. However, given the basic nature of the above result, one may wonder whether the same answer could have been obtained based on simpler evolution methods, such as the “pure” TEBD algorithm without any truncation from DAOE. After all, in the free-fermion limit $\Delta = 0$, the system’s entanglement remains low for all times, which is the regime in which TEBD is expected to be efficient. In Fig. 3(b) we test this notion by plotting $\Delta^2 D(\Delta^2 t)$ as calculated from TEBD simulations against the same fDAOE data shown in Fig. 3(a): we find that for all Δ , truncation errors accumulate significantly before the evolution reaches the crossover timescale $\Delta^2 t = 1$ and TEBD fails catastrophically, with $D(t)$ nosediving toward unphysical negative values. We note that while the bond dimension used for TEBD (128, compared to 96 for fDAOE) is relatively low, to completely avoid truncation errors the required bond dimension must grow exponentially in time. The success of DAOE for simulating long times lies in the fact that the required bond dimension is bounded for all times by a value controlled by the dissipation parameters.

Thus, fDAOE allows us to efficiently reach diffusive timescales that remain unavailable to more standard methods.

We make two additional observations from the data in Fig. 4(b): first, observe that for the larger Δ , $D(t)$ exhibits strong plateaus (in $1/t$) toward the final value (visible for the three largest Δ). This is unexpected, as the hydrodynamic theory would predict power law tails as we discuss in Sec. V; see also [30,31]. We do not have a satisfying explanation of this; it might be an artifact of the fDAOE dissipator suppressing hydrodynamic tails, or those tails might just be small in this system.

Second, we note that the predicted diffusion constant generally *increases* as the parameter γ is increased. At first glance this is also somewhat surprising, as dissipation (such as between the system and an environment) is generally expected to lead to increased loss of coherence and faster approach to diffusion. We provide a heuristic interpretation of this behavior as akin to a dissipation-induced “diffusive Zeno effect”: when $\ell_* = 2$, fDAOE acts to suppress growth of larger fermion strings, while leaving quadratic strings invariant. It is easy to see that for $\gamma \rightarrow \infty$, interactions are completely blocked and no diffusive transport can occur. For large γ , fermions remain “confined” within the quadratic free-fermion space and charge continues to be transported ballistically for long times. We show additional results for this effect in Appendix C.

V. FERMI’S GOLDEN RULE, AND AN OPERATOR-SPREADING PICTURE FOR THE DIFFUSIVE CROSSOVER

Our numerical simulations suggest that the ballistic-diffusive crossover time and diffusion constant both scale as Δ^{-2} . Here we show that the same scaling is obtained perturba-

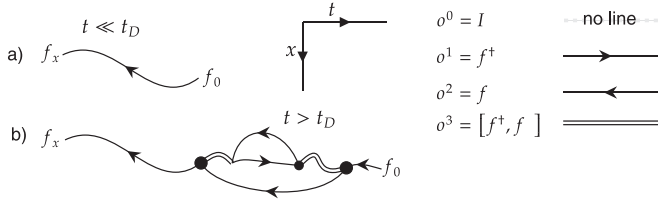


FIG. 5. An operator path integral for the single-particle Green's function $G(x, t) = \langle f_x(t) | f_0 \rangle$ consists of a sum of operator trajectories starting at f_x on the left, and evolving to f_0 at time t . (a) In the absence of interactions, the number of fermion operators is conserved, and this remains approximately true at early times when interactions are unimportant. (b) At later times, interactions cause 1-body operators to grow in Fermi weight, which leads to an (exponential in time) suppression of the amplitude $G(x, t)$.

tively using a Fermi's golden rule style of argument. We first argue that the lifetime of a single-fermion Green's function goes as Δ^{-2} , and then use that result to deduce that the diffusion constant has the same scaling. However, this argument is ultimately uncontrolled in ways we discuss, showing the need for the numerical methods developed above.

Along the way it is useful to interpret the ballistic-diffusive crossover in an operator-spreading picture [11], which we now introduce. The correlation functions used to determine the diffusion constant can all be written as inner products on the space of operators $\langle A(t) | B \rangle$ where A, B are operators, and A is evolved in the Heisenberg picture. This inner product is a quantum transition amplitude in the space of operators (rather than the more familiar space of states). It is the amplitude for an operator A to Heisenberg-evolve to an operator B at a time t . By Trotterizing the Heisenberg time evolution and inserting a complete set of states, we can express $\langle A(t) | B \rangle$ as a sum over operator histories (see Fig. 5 for an illustration of some such histories). Each history has the same boundary condition: The initial/final configurations are A, B respectively. In the present case, a complete set of states can be represented by a string $o^\mu \equiv \otimes_r o_r^\mu$, where $o^{0,1,2,3} = I, f^\dagger, f, [f^\dagger, f]$ is a complete on-site basis of operators. The fermion creation/annihilation operators $o^{1,2}$ are represented by horizontal lines with orientations \rightarrow, \leftarrow respectively. On the other hand $o^3 = 1 - 2n$ is represented by a double line (a natural notation given that it is bilinear in fermion operators). o^0 is represented by the absence of a line (Fig. 5). There are rules constraining the allowed histories. For example, unitarity implies the lines cannot start or end in a region of I 's. U(1) symmetry implies that difference between the number of f 's and f^\dagger 's remains constant in time.

In the absence of interactions, the f, f^\dagger operators evolve into a linear superposition of single f, f^\dagger operators respectively, according to the equation Eq. (4). This is a property special to quadratic Hamiltonians. In the corresponding operator-spreading picture, this means that one only need sum over histories where a single-fermion operator changes position [Fig. 5(a)]. In the presence of interactions new operator histories become relevant, where the number of operator world lines increases or decreases [Fig. 5(b)], and the histories become more “complicated” in a sense we describe shortly.

We now argue that there is a Δ^{-2} timescale associated with fermion operators becoming more complicated. To be more precise, consider the Green's function $G(x, t) \equiv \langle f_x(t) | f_0(0) \rangle$. This transition amplitude is associated with operator histories that begin with f at position x and end with an f at position 0 at time t . In the absence of interactions $G^{(0)}(x, t) = K(x, t)$ behaves ballistically; it is supported in a region $|x| < vt$, and has typical size $1/\sqrt{t}$, consistent with a sum rule $\sum_x |G^{(0)}(x, t)|^2 = 1$. The corresponding simple operator histories are shown in Fig. 5(a). However in the presence of interactions, the Green's function is expected to decay much faster (indeed, exponentially) with time [32], and this is associated with the appearance of more complicated diagrams, Fig. 5(b). The reasoning (see [11]) is that once operators are allowed to branch, the initial operator f_x is much more likely to grow in Fermi weight than it is to end up as the Fermi weight 1 operator f_0 , which implies that the transition amplitude/Green's function decays in time.

We conjecture that in the presence of interactions, the Green's function decays exponentially as $G(x, t) \sim e^{-O(\Delta^2 t)}$. We can argue for this using the *memory matrix* (MM) formalism [6]. In the MM formalism, one divides the set of observables into two categories, “fast” and “slow” modes. In our case, we choose the latter to be linear combinations of single-fermion operators; the fast space is taken to be the orthogonal complement to the slow space. One can then derive an exact equation of motion for G in momentum space [6] which takes the following form:

$$\partial_t G_k - im_k G_k + \int_0^t ds \Sigma_k(s) G_k(t-s) = 0. \quad (9)$$

Here, m_k represents the free (quadratic) part of the dynamics, such that $[H_0, f_k] = -m_k f_k$.³ $\Sigma_k(s)$ represents a memory term, arising from operators leaving and then later reentering the slow subspace. It is defined as

$$\Sigma_k(s) = \langle f_k | L Q e^{-iQLQs} Q L | f_k \rangle, \quad (10)$$

where $L = [H, \cdot]$ is the many-body Liouvillian generating the dynamics in the Heisenberg picture, and Q is the projector onto the fast space. Using the fact that the noninteracting terms do not induce any transitions from slow to fast operators, we can further simplify the above expression to

$$\Sigma_k(s) = \Delta^2 \Gamma_k(s) \equiv \Delta^2 \langle [V, f_k] | Q e^{-iQLQs} Q [V, f_k] \rangle,$$

where V is the interaction term and Δ is the interaction strength appearing in the Hamiltonian Eq. (7). It is readily verified that $[V, f_k]$ is a 3-fermion operator; therefore $\Gamma_k(s)$ is a 3-fermion autocorrelation function with dynamics constrained to the fast space (i.e., dynamics generated by QLQ). Since Γ_k only involves dynamics in the fast subspace, we expect that it decays quickly in time. Putting this together, we have

$$\partial_t G_k - im_k G_k + \Delta^2 \int_0^t ds \Gamma_k(s) G_k(t-s) = 0. \quad (11)$$

³Our Hamiltonian has unit cell of size 2, so m, G, Γ, Σ are each 2×2 matrices, and f_k, f_k^\dagger also carry sublattice indices. We suppress the corresponding sublattice index, which is unimportant for our discussion. Note m_k is a Hermitian matrix.

A Fermi's golden rule scaling emerges from this equation of motion if Γ_k decays over a timescale κ^{-1} that is independent of interactions in the small- Δ limit. This allows one to truncate the integral in Eq. (11) to obtain

$$\partial_t G_k - im_k G_k + \frac{\Delta^2}{\kappa} G_k \approx 0. \quad (12)$$

This implies $\partial_t |G_k|^2 \approx -\frac{2\Delta^2}{\kappa} |G_k|^2$, so that the single-fermion operators have a lifetime scaling as Δ^{-2} , in agreement with the data presented in Fig. 3.

In fact, this argument is delicate, especially in 1D. It turns out that in the noninteracting approximation⁴ the 3-fermion correlator decays as $|\Gamma_k(s)| \sim 1/s$ (consistent with dimension counting), which is not sufficiently quick to safely truncate the time integral. A self-consistent resolution to this issue is to include the effects of interactions on Γ through the ansatz $|\Gamma_k(s)| \sim e^{-c\Delta^2 s}/s$, which has the expected $1/s$ decay at early times, and the expected exponential decay at later times. This ansatz leads to the advertised FGR lifetime for G_k but with a weak additional logarithmic dependence $|G_k(t)| \sim e^{-O(\Delta^2 \log(\Delta^{-1}t))}$. Our numerical data are insufficiently resolved to confirm or exclude such subtle logarithmic corrections, so henceforth we will ignore them here.⁵

The uncontrolled argument above suggests that that fermion operators propagate freely and ballistically up until time $t_G \sim 1/\Delta^2$, past which interactions become important. In the operator-spreading language, the world lines of fermion operators become complicated on said timescale. What are the consequences for the diffusion constant? Conflating t_G with a mean free time for particle collisions, and substituting the result into the Drude formula, we expect the diffusion constant to also scale as t_G .

In what follows we make a more explicit argument that $D \sim t_G$. We start from the Kubo formula for the diffusion constant, and evaluate it using an operator-spreading picture and the above results. We argue that the time derivative of the diffusion constant $\dot{D}(t)$ is $O(1)$ early times $t \lesssim t_G$, but starts to decay algebraically once $t \gtrsim t_G$. As a result $D(t) = D + \text{poly}(t^{-1})$ at late times, where D scales as t_G . The Kubo formula [equivalent to Eq. (1) in the thermodynamic limit] implies that the time derivative of $D(t)$, as defined in Eq. (1), is $\dot{D}(t) = \langle \mathcal{J}(t) | \mathcal{J}(0) \rangle / L$, where \mathcal{J} is the total current $\mathcal{J} = \sum_x [i f_x^\dagger f_{x+1} + \text{H.c.}] = \sum_x j_x$, which is quadratic in fermion operators. Therefore $\dot{D}(t)$ involves a sum of correlations of the form

$$\langle (f_x^\dagger f_{x+1})(t) | f_y^\dagger f_{y+1} \rangle. \quad (13)$$

This expression can be read as a propagator in the space of operators; it represents the amplitudes for the operators $f_x^\dagger f_{x+1}$ to end up in the configuration $f_y^\dagger f_{y+1}$ at time t under Heisenberg dynamics (Fig. 6).

⁴Obtained by replacing QLQ with QL_0Q in the definition of Γ where $L_0 = [H_0, \cdot]$.

⁵For more details, see the forthcoming work by von Keyserlingk *et al.* [33].

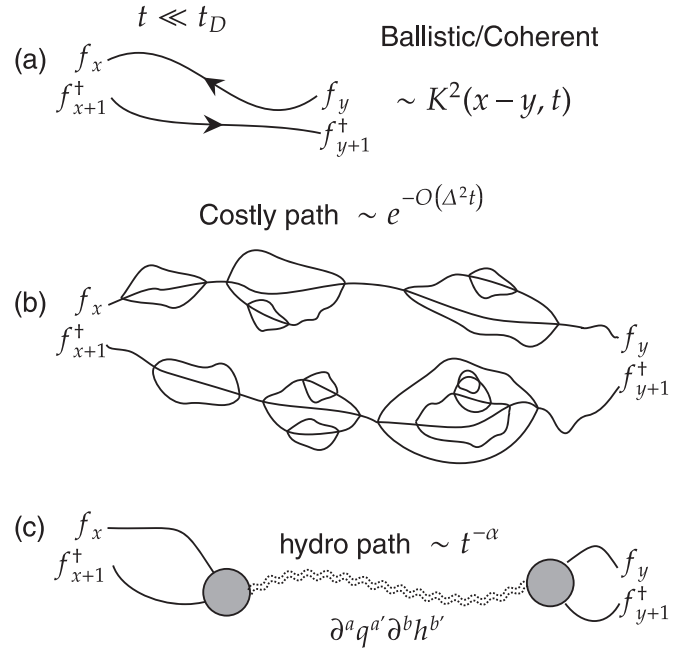


FIG. 6. A diagram of contributions to the current-current correlator. (a) At early times, the dominant contribution to transport comes from paths where the fermion operators do not grow in Fermi weight but instead ballistically spread according to the noninteracting dynamics. We identify two sorts of paths at later times. (b) Those paths where the initial fermions propagate independently, but undergo forking events due to interactions are expected to decay exponentially. (c) Paths where the fermions combine into a hydrodynamic operator (local charge n and energy h densities, and their derivatives) are expected to decay as a power law according to hydrodynamics. Contributions of type (c) are expected to dominate at late times.

At early times, interactions are unimportant and each f, f^\dagger making up j_x evolves according to Eq. (4). In this case, a straightforward analysis of the propagator K (which corresponds to coherent/ballistic dynamics of the fermion operators) shows that $\langle j_x(t) j_y \rangle \sim 1/t$ for $|x-y| < vt$, which implies $\dot{D}(t)$ is $O(1)$ at early times. Thus $D(t)$ grows linearly in t at early times. In the operator-spreading picture, the fermion operators spread independently and ballistically in this regime, undergoing essentially no branching events [Fig. 6(a)].

However at later times interactions become important, and the fermion operators comprising \mathcal{J} branch into more complicated superpositions of higher Fermi weight operators [Fig. 6(b)]. As mentioned above, this process is difficult to reverse (in ergodic systems) [11]. So the amplitude that f_x^\dagger, f_{x+1} separately evolve to f_y^\dagger, f_{y+1} while having many branching events in the interim [Fig. 6(b)] ends up decaying exponentially in time as $e^{-O(t/t_G)}$. In other words, the world lines of each fermion operator in the expressions for $\dot{D}(t)$ become costly; they develop a linear line tension.

In this later-time regime, a different class of operator history becomes dominant: the paths where the fermion operators making up j_x coalesce into hydrodynamical variables [Fig. 6(c)]; these operators decay more slowly (as a power law in time, rather than exponentially), and so effectively

have a lower line tension.⁶ The simplest and most relevant hydrodynamical operators in ergodic systems involve products and derivatives of the local energy (ε) and charge (n) densities of the form $\partial_x^a n^a \partial_x^b \varepsilon^b$. The ones relevant to this discussion are $\varepsilon \partial_x n$, $\varepsilon^2 \partial_x n$, \dots , although which of these are present can generally depend on discrete symmetries, filling, and temperatures [30,34]. These operators have less costly world lines, because of the underlying local conservation laws, and their correlations decay as power laws $1/t^\alpha$ rather than exponentially.⁷ We expect the crossover time (where both types of path balance) to obey $e^{-t/t_G} \sim C/t^\alpha$, consistent with crossover $t_D \sim t_G$ with possible logarithmic enhancements. In conclusion, we expect $\dot{D}(t) = O(1)$ until a time $O(t_G)$ at which point $\dot{D}(t)$ will start to decay as a power law. This suggests that $D \sim 1/\Delta^2$ as expected, and that $D(t)$ approaches this final value as a power law $1/t^{\alpha-1}$.

VI. CONCLUSIONS

We investigated the transport of interacting one-dimensional fermions using a numerical scheme that we developed building on the earlier DAOE method [7]. This method, which we named fDAOE, evolves fermionic observables in time, applying to them a truncation which discards observables that involve large numbers of creation/annihilation operators, thus making the dynamics tractable. In one dimension, this truncation scheme has a simple representation in a matrix product operator language, which allows for efficient numerical simulations.

Unlike the existing DAOE method, fDAOE is exact for free fermions, and we presented numerical evidence that it is able to correctly capture long-time transport properties for a range of interaction strengths. In particular, we focused on a regime where interactions are weak, which results in parametrically long timescales that are difficult to simulate using brute force approaches. We showed that fDAOE can overcome this limitation, and obtain the expected crossover from ballistic to diffusive transport. We used fDAOE to extract both the crossover timescale and the value of the diffusion constant, both scaling as Δ^{-2} with the interaction strength Δ . We further justified this scaling by outlining a perturbative Fermi's golden rule calculation, suggesting that it is at this $O(\Delta^{-2})$ timescale that the free-fermion approximation breaks down. We also provided an operator-spreading picture of the crossover to the late-time diffusive regime.

Our results open the way toward more thorough investigations of charge transport in interacting fermionic systems. There are various directions in which the method could be further extended to bring it closer to describing experimentally relevant systems. One obvious extension would be to two-dimensional systems. Here, MPS methods are routinely used to study the quasi-1D limit of thin cylinders [35]: time

evolution of genuine 2D systems is hard because the bond dimensions for the associated MPOs typically scale with the cylinder width [36]. However, as mentioned in Sec. II, the fDAOE MPO has a constant bond dimension independent of the spatial dimension, so this step does not entail additional complexity. Applying the 2D fDAOE to spinful fermions (as described in Sec. II) could allow study of the paradigmatic 2D Hubbard model [37], for example. Another open problem is to extend the validity of fDAOE from the infinite-temperature limit we considered to finite temperatures and study its effect on transport. Finally, one could consider including interactions with phonons [38].

Note added. We would like to bring the reader's attention to a related, independent work of Kuo *et al.* [39].

ACKNOWLEDGMENTS

We thank Romain Vasseur, Sarang Gopalakrishnan, Iliya Essin, Chaitanya Murthy, and Alex Michailidis for useful conversations. C.v.K. is supported by UKRI Future Leaders Fellowship No. MR/T040947/1. T.R. is supported in part by the Stanford Q-Farm Bloch Postdoctoral Fellowship in Quantum Science and Engineering. This research was in parts financially supported by the European Research Council (ERC) under the European Union's Horizon 2020 research and innovation program under Grant Agreement No. 771537. F.P. acknowledges the support of the Deutsche Forschungsgemeinschaft (DFG, German Research Foundation) under Germany's Excellence Strategy EXC-2111-390814868 and DFG Research Unit FOR 5522 (Project ID 499180199). F.P.'s research is part of the Munich Quantum Valley, which is supported by the Bavarian state government with funds from the Hightech Agenda Bayern Plus.

APPENDIX A: SPIN AND FERMION DAOE AT FINITE Δ

The fermionic DAOE method is expected to correctly capture transport dynamics for models with approximate long-lived fermionic quasiparticles, as argued in Sec. V. In contrast, the spin DAOE method of Ref. [7] fails to capture even the free-fermion limit ($\Delta = 0$) of the model in Eq. (7), as we showed in Fig. 1. It is natural to ask at what point the fermion nature of the problem is lost and it becomes practical to use the spin DAOE method. We know, for example, that certain spin models (e.g., the spin ladder model studied in Ref. [7]) can be accurately studied using spin DAOE even though they admit local fermionic descriptions.

To answer this question, in Fig. 7 we compare the time-dependent diffusion constants for the model of Eq. (7), for both spin and fermion DAOE methods. We show results for three interaction strengths ranging from weak to strong interactions, $\Delta = 0.01, 0.1, 1$. The system size is $L = 100$; otherwise parameters are the same as in Fig. 3(a). Results are for bond dimension $\chi = 96$; for $\Delta = 1$ we show data also at $\chi = 192$ to ascertain convergence. For weak interactions ($\Delta = 0.01, 0.1$), we observe a clear disparity between fermion and spin algorithms. The former show the extended period of ballistic behavior which is expected on physical grounds, while the latter rapidly revert to diffusion. For $\Delta = 1$, the two methods are in approximate agreement, predicting a rapid

⁶Here it is important that j has a charge-neutral component; otherwise it would not be able to develop an overlap with hydrodynamical slow modes [11]. This is ultimately the reason why $\langle j_x(t) | j_y \rangle$ correlators decay as a power law, while the single-particle Green's function $\langle f_x(t) | f_y \rangle$ decays exponentially.

⁷One always finds $\alpha \geq 3/2$ [11,30,34].

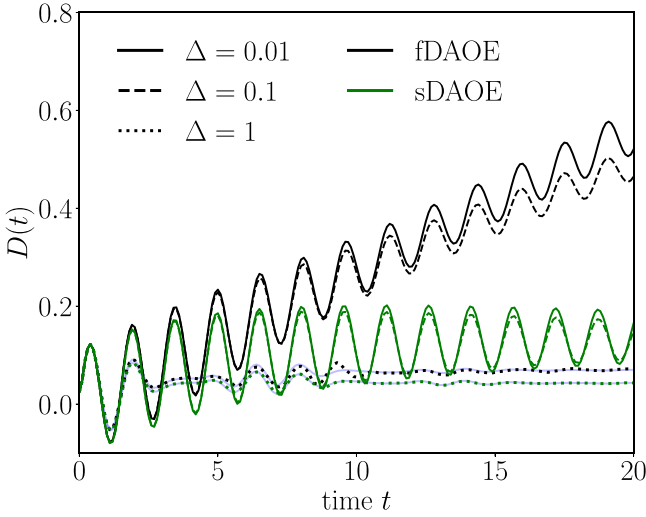


FIG. 7. Time-dependent diffusion constant $D(t)$ vs time t , comparing fermion DAOE (fDAOE) and spin DAOE (sDAOE) for different interaction strengths Δ . System size $L = 100$, DAOE parameters $\gamma = 0.1$, $\ell_* = 2$, and bond dimension $\chi = 96$. Spin DAOE fails to capture the ballistic dynamics for small Δ , but is consistent with fermion DAOE in the strongly interacting regime $\Delta = O(1)$. For $\Delta = 1$ we show additional data with $\chi = 192$ (light blue)

onset of diffusive dynamics. Note, however, that a quantitative comparison of the two methods only makes sense in the $\gamma \rightarrow 0$ limit.

These results agree with our intuition that spin DAOE is less efficient than fDAOE at capturing transport in regimes with long-lived fermionic quasiparticles, which in the present case are responsible for the extended period of ballistic behavior. Here by less efficient we mean that spin DAOE will require a smaller γ (and consequently more memory) to capture the relevant ballistic physics, which is encoded in operators with long Jordan-Wigner strings (see Sec. II). However both fDAOE and spin DAOE perform similarly when the quasiparticles have short lifetimes, for example when the strength of fermion interaction terms becomes comparable

to that of the noninteracting terms. The spin ladder model in Ref. [7] in fact contains $O(1)$ density-dependent hopping terms, in the fermion language, which explains why the spin algorithm produced physically meaningful results in that case.

APPENDIX B: CONVERGENCE WITH BOND DIMENSION AND ℓ_*

Here we report additional data for different ℓ_* and different bond dimensions $\chi = 64, 96, 128$ ($\ell_* = 2$) and $\chi = 256, 512$ ($\ell_* = 4$). In Fig. 8 we plot the time-dependent diffusion constant $D(t)$ for $\ell_* = 2$ and different bond dimensions, for $\gamma = 0.03$ in Fig. 8(a) and $\gamma = 0.05$ in Fig. 8(b). We show data for the four largest Δ considered in the main text: for decreasing Δ , or increasing γ , entanglement growth is reduced and errors are smaller. We see clear evidence of truncation error for $\chi = 64$, $\Delta = 0.1$, and $\gamma = 0.03$ at early times, as expected. However, even in this case, the late-time diffusive dynamics is well converged with the larger bond dimension $\chi = 128$ results. The diffusive transport appears to “recover” from early-time errors as DAOE continuously suppresses entanglement growth.

We show the same data but for $\ell_* = 4$ in Fig. 9. Here the story is similar although the truncation errors are larger; this is expected, because increasing ℓ_* implies that that higher weight operators (specifically, with Fermi weight ≤ 4) are kept rather than discarded, and thus more entanglement can be generated. Given the large bond dimensions (256 and 512), we are limited to shorter times and it is difficult to assess the convergence for late times. Note that we do not use the $\ell_* = 4$ data anywhere in the main text, but these results act as a check on whether our $\ell_* = 2$ results are sensible.

The data for different ℓ^* are not necessarily expected to agree for finite γ . To compare the two cases, we plot $D(t)$ curves extrapolated with a quadratic fit in $\gamma \rightarrow 0$, in Fig. 10, for $\chi = 128$ ($\ell_* = 2$) and $\chi = 256$ ($\ell_* = 4$). For $\Delta \neq 0.1$ we extrapolate in $\gamma \in (0.03, 0.05, 0.1, 0.2)$, while for $\Delta = 0.1$ we ignore the 0.03 data point, due to the visible truncation effects in Figs. 8 and 9. We obtain a reasonable quantitative

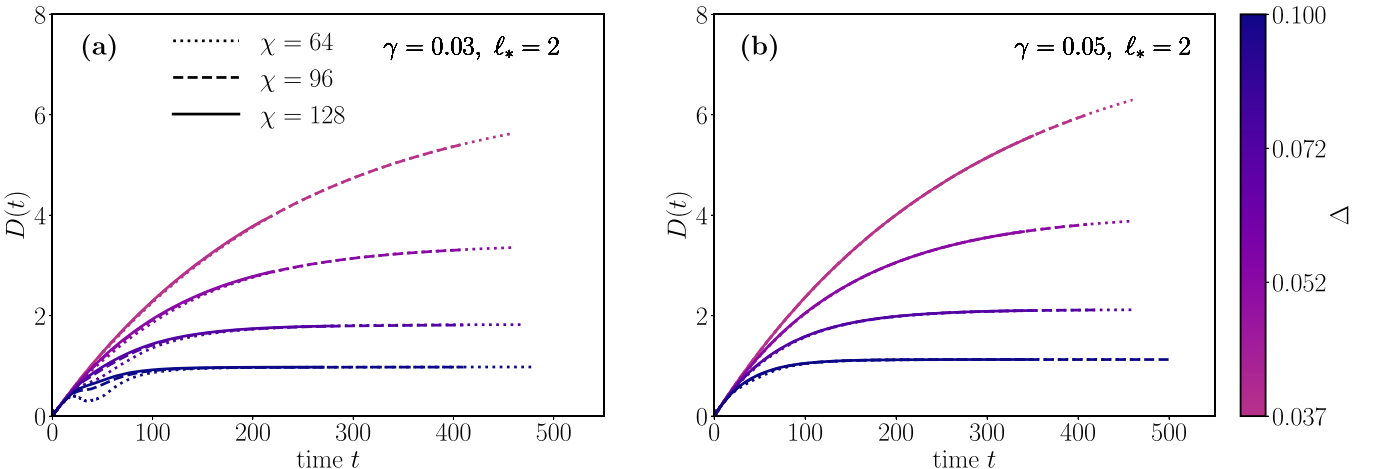


FIG. 8. (a) For $\ell_* = 2$, we plot $D(t)$ for different bond dimensions, $\chi = 64$ (dotted line), $\chi = 96$ (dashed), $\chi = 128$ (solid), and $\gamma = 0.03$. For larger Δ , the data are less well converged at early times, but converged at late times in the diffusive regime. (b) Same plot for $\gamma = 0.05$.

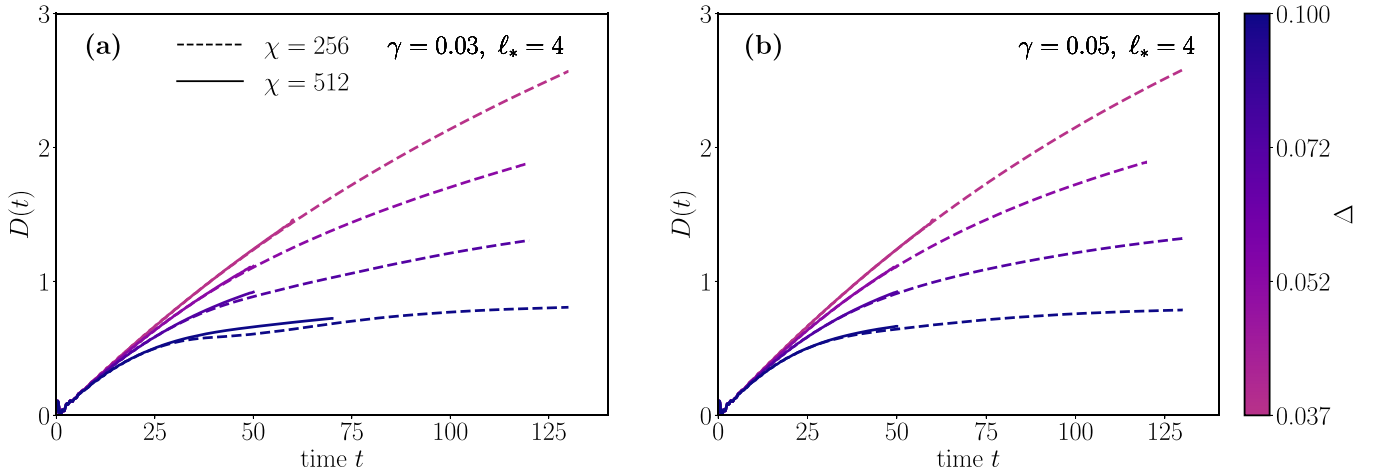


FIG. 9. (a) For $l_* = 4$, same as Fig. 8 with $\chi = 256$ (dashed line), $\chi = 512$ (solid), and $\gamma = 0.03$. The convergence is slightly worse compared to the $l_* = 2$ case. (b) Same plot for $\gamma = 0.05$.

convergence; i.e., the difference between $l_* = 2, 4$ is much smaller than the difference between different Δ .

We conclude that the data used in the main text ($\chi = 96$, $l_* = 2$) are reasonably well converged in bond dimension, and the extrapolated diffusion constants in Fig. 4 are not seriously affected by truncation errors or the small l^* cutoff.

APPENDIX C: ENTANGLEMENT DYNAMICS AND DIFFUSIVE ZENO EFFECT

In this Appendix we study the dynamics of operator space entanglement entropy (OSSE) growth under fDAOE, and give an argument for the “diffusive Zeno effect” mentioned in the main text.

We bipartition the system into left and right subsystems A ($x < 0$) and B ($x \geq 0$), and define the (half chain) operator entanglement of a Heisenberg-evolved operator $q(t)$ as

$$S_{vN}[q] = -\text{Tr}(\rho_A^q \log \rho_A^q), \quad (\text{C1})$$

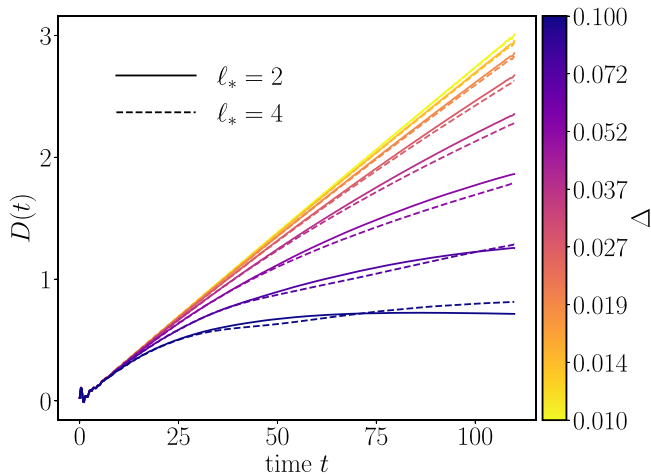


FIG. 10. $D(t)$ for $l_* = 2$, $\chi = 128$ (solid lines) vs $l_* = 4$, $\chi = 256$ (dashed lines), for the different Δ used in the main text. The $D(t)$ curves are extrapolated in $\gamma \in (0.03, 0.05, 0.1, 0.2)$ for $\Delta \neq 0.1$ and $\gamma \in (0.05, 0.1, 0.2)$ for $\Delta = 0.1$, due to the larger truncation errors for $\gamma = 0.03$ and $\Delta = 0.1$.

where ρ_A^q is the “density operator” of the vectorized MPS representation of q after tracing out B , i.e.,

$$\rho_A^q = \text{Tr}_B(|q\rangle\langle q|). \quad (\text{C2})$$

Under generic unitary evolution, the entanglement grows linearly in time, and storing this highly entangled state is the main obstacle to “exact” evolution schemes like TEBD. Applying the DAOE dissipator decreases this entanglement, and its late-time value remains bounded by a cutoff depending on the parameters l_* and γ . This suppression is the reason for the success of DAOE in simulating long-time transport [7,11].

In Fig. 11 we plot the half-chain OSSE (normalized by $\log 2$) for the time-evolved operators $q_0(t) = \sigma_0^z(t)$ we study in the main text, for different Δ . The solid lines are with $l_* = 2$ and the dotted lines with $l_* = 4$, $\gamma = 0.03$ in the main figure. We observe a linear growth toward the value $S_{vN} \approx$

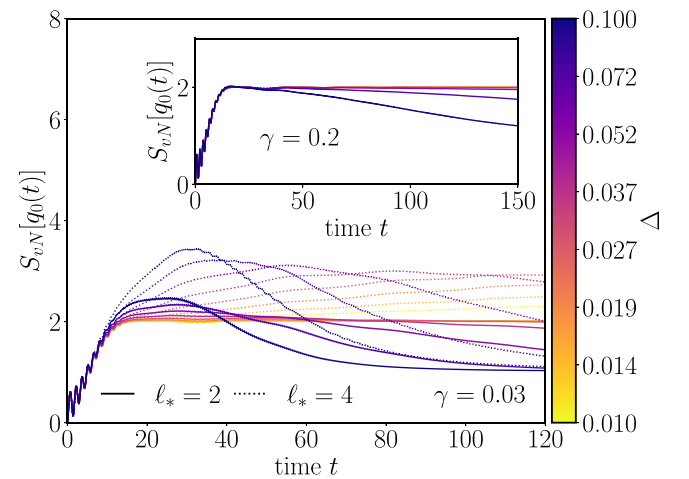


FIG. 11. Half chain operator entanglement growth for $\gamma = 0.03$ and $l_* = 2$ (solid lines), $l_* = 4$ (dotted lines). Entanglement rapidly approaches a $2 \log 2$ plateau, before slowly increasing at a rate set by Δ (for $l_* = 4$) and eventually decreasing toward $\log 2$ due to the DAOE dissipation. Inset: Entanglement growth for $\gamma = 0.2$. The stronger dissipation leads to frozen dynamics, with entanglement decaying more slowly compared to the $\gamma = 0.03$ case.

$2 \log 2$, after which the entanglement dynamics depends on ℓ_* and the interaction strength Δ . For $\ell_* = 2$, the entanglement plateaus around the value $2 \log 2$ up to a timescale that decreases with Δ , before slowly decaying to $S_{vN} = \log 2$ consistent with diffusion [7]. The plateau can be understood as arising from the noninteracting physics as follows: σ_x^z is bilinear in fermion operators; at early times, the two fermion operators essentially evolve under free dynamics, each becoming a superposition of single fermions within a light cone. Each of these fermion operators has entropy $\sim \log 2$ across the central cut, and the entropy of their product $\sigma_x^z(t)$ is approximately the sum of their entropies, namely $2 \log 2$. The decay then follows as weight is slowly converted through interactions into higher weight terms, which fDAOE removes.

For $\ell_* = 4$, operators are allowed to grow into larger strings (of Fermi weight 4) before truncation begins. This leads to a growth of entanglement away from the $2 \log 2$ plateau, with faster rate of entanglement production for larger Δ . At late times, DAOE overcomes the rate of entanglement

generation and S_{vN} falls again toward the expected $\log 2$ asymptotic value [7].

We now discuss why the diffusion constant is observed to increase with γ , as we show in the inset to Fig. 4. Again, a naive picture of DAOE as “dissipation” would suggest that the method destroys the system coherence and stabilizes diffusion. In the inset to Fig. 11 we plot the OSEE growth for $\ell_* = 2$, but now for larger $\gamma = 0.2$. The entanglement is essentially “frozen” at the free-fermion entanglement value $S_{vN} = 2 \log 2$, with the entanglement in the case of strong Δ decaying much slower than for the smaller γ case. When the dissipation is strong, the operator is prevented from ever leaving the free-fermion subspace of length $\ell = 2$ operators. This can be interpreted as a freezing of the interactions, $\Delta \rightarrow 0$, which leads to a diverging diffusion constant and purely ballistic dynamics in the limit $\gamma \rightarrow \infty$. We dub this phenomena the “diffusive Zeno effect” as it is suggestive of the phenomena where a repeatedly measured state exhibits frozen evolution.

-
- [1] L. D’Alessio, Y. Kafri, A. Polkovnikov, and M. Rigol, From quantum chaos and eigenstate thermalization to statistical mechanics and thermodynamics, *Adv. Phys.* **65**, 239 (2016).
- [2] T. Rakovszky, F. Pollmann, and C. W. von Keyserlingk, Diffusive hydrodynamics of out-of-time-ordered correlators with charge conservation, *Phys. Rev. X* **8**, 031058 (2018).
- [3] V. Khemani, A. Vishwanath, and D. A. Huse, Operator spreading and the emergence of dissipative hydrodynamics under unitary evolution with conservation laws, *Phys. Rev. X* **8**, 031057 (2018).
- [4] D. E. Parker, X. Cao, A. Avdoshkin, T. Scaffidi, and E. Altman, A universal operator growth hypothesis, *Phys. Rev. X* **9**, 041017 (2019).
- [5] A. Lucas, Operator size at finite temperature and Planckian bounds on quantum dynamics, *Phys. Rev. Lett.* **122**, 216601 (2019).
- [6] D. Forster, *Hydrodynamic Fluctuations, Broken Symmetry, and Correlation Functions* (CRC Press, Boca Raton, FL, 2018).
- [7] T. Rakovszky, C. W. von Keyserlingk, and F. Pollmann, Dissipation-assisted operator evolution method for capturing hydrodynamic transport, *Phys. Rev. B* **105**, 075131 (2022).
- [8] T. Klein Kvorning, L. Herviou, and J. H. Bardarson, Time-evolution of local information: Thermalization dynamics of local observables, *SciPost Phys.* **13**, 080 (2022).
- [9] C. Artiago, C. Fleckenstein, D. Aceituno, T. K. Kvorning, and J. H. Bardarson, Efficient large-scale many-body quantum dynamics via local-information time evolution, [arXiv:2310.06036](https://arxiv.org/abs/2310.06036).
- [10] C. D. White, Effective dissipation rate in a Liouvillian-graph picture of high-temperature quantum hydrodynamics, *Phys. Rev. B* **107**, 094311 (2023).
- [11] C. von Keyserlingk, F. Pollmann, and T. Rakovszky, Operator backflow and the classical simulation of quantum transport, *Phys. Rev. B* **105**, 245101 (2022).
- [12] S. A. Hartnoll and A. P. Mackenzie, Colloquium: Planckian dissipation in metals, *Rev. Mod. Phys.* **94**, 041002 (2022).
- [13] H. Ott, E. de Mirandes, F. Ferlino, G. Roati, G. Modugno, and M. Inguscio, Collisionally induced transport in periodic potentials, *Phys. Rev. Lett.* **92**, 160601 (2004).
- [14] S. Scherg, T. Kohlert, J. Herbrych, J. Stolpp, P. Bordia, U. Schneider, F. Heidrich-Meisner, I. Bloch, and M. Aidelsburger, Nonequilibrium mass transport in the 1D Fermi-Hubbard model, *Phys. Rev. Lett.* **121**, 130402 (2018).
- [15] M. A. Nichols, L. W. Cheuk, M. Okan, T. R. Hartke, E. Mendez, T. Senthil, E. Khatami, H. Zhang, and M. W. Zwierlein, Spin transport in a Mott insulator of ultracold fermions, *Science* **363**, 383 (2019).
- [16] P. T. Brown, D. Mitra, E. Guardado-Sanchez, R. Nourafkan, A. Reymbaut, C.-D. Hébert, S. Bergeron, A.-M. S. Tremblay, J. Kokalj, D. A. Huse, P. Schauß, and W. S. Bakr, Bad metallic transport in a cold atom Fermi-Hubbard system, *Science* **363**, 379 (2019).
- [17] N. W. Ashcroft and N. D. Mermin, *Solid State Physics* (Cengage Learning, Boston, MA, 2022).
- [18] U. Schollwöck, The density-matrix renormalization group in the age of matrix product states, *Ann. Phys.* **326**, 96 (2011).
- [19] S. Paeckel, T. Köhler, A. Swoboda, S. R. Manmana, U. Schollwöck, and C. Hubig, Time-evolution methods for matrix-product states, *Ann. Phys.* **411**, 167998 (2019).
- [20] T. Prosen and M. Žnidarič, Is the efficiency of classical simulations of quantum dynamics related to integrability? *Phys. Rev. E* **75**, 015202(R) (2007).
- [21] C. Jonay, D. A. Huse, and A. Nahum, Coarse-grained dynamics of operator and state entanglement, [arXiv:1803.00089](https://arxiv.org/abs/1803.00089).
- [22] T. Prosen and I. Pižorn, Operator space entanglement entropy in a transverse Ising chain, *Phys. Rev. A* **76**, 032316 (2007).
- [23] G. Vidal, Efficient classical simulation of slightly entangled quantum computations, *Phys. Rev. Lett.* **91**, 147902 (2003).
- [24] C. Hess, Heat conduction in low-dimensional quantum magnets, *Eur. Phys. J.: Spec. Top.* **151**, 73 (2007).

- [25] D. Hirobe, M. Sato, T. Kawamata, Y. Shiomi, K.-i. Uchida, R. Iguchi, Y. Koike, S. Maekawa, and E. Saitoh, One-dimensional spinon spin currents, *Nat. Phys.* **13**, 30 (2017).
- [26] B. Bertini, F. Heidrich-Meisner, C. Karrasch, T. Prosen, R. Steinigeweg, and M. Žnidarič, Finite-temperature transport in one-dimensional quantum lattice models, *Rev. Mod. Phys.* **93**, 025003 (2021).
- [27] G. M. Crosswhite and D. Bacon, Finite automata for caching in matrix product algorithms, *Phys. Rev. A* **78**, 012356 (2008).
- [28] Y. Huang, C. Karrasch, and J. E. Moore, Scaling of electrical and thermal conductivities in an almost integrable chain, *Phys. Rev. B* **88**, 115126 (2013).
- [29] J. Hauschild and F. Pollmann, Efficient numerical simulations with tensor networks: Tensor network Python (TeNPy), *SciPost Phys. Lect. Notes* **5**, (2018).
- [30] S. Mukerjee, V. Oganesyan, and D. Huse, Statistical theory of transport by strongly interacting lattice fermions, *Phys. Rev. B* **73**, 035113 (2006).
- [31] A. A. Michailidis, D. A. Abanin, and L. V. Delacrétaz, Corrections to diffusion in interacting quantum systems, [arXiv:2310.10564](https://arxiv.org/abs/2310.10564).
- [32] A. Bohrdt, C. B. Mendl, M. Endres, and M. Knap, Scrambling and thermalization in a diffusive quantum many-body system, *New J. Phys.* **19**, 063001 (2017).
- [33] C. von Keyserlingk *et al.* (unpublished).
- [34] X. Chen-Lin, L. V. Delacrétaz, and S. A. Hartnoll, Theory of diffusive fluctuations, *Phys. Rev. Lett.* **122**, 091602 (2019).
- [35] E. M. Stoudenmire and S. R. White, Studying two-dimensional systems with the density matrix renormalization group, *Annu. Rev. Condens. Matter Phys.* **3**, 111 (2012).
- [36] M. P. Zaletel, R. S. K. Mong, C. Karrasch, J. E. Moore, and F. Pollmann, Time-evolving a matrix product state with long-ranged interactions, *Phys. Rev. B* **91**, 165112 (2015).
- [37] J. Hubbard, Electron correlations in narrow energy bands, *Proc. R. Soc. London A* **276**, 238 (1963).
- [38] C. Brockett, F. Dorfner, L. Vidmar, F. Heidrich-Meisner, and E. Jeckelmann, Matrix-product-state method with a dynamical local basis optimization for bosonic systems out of equilibrium, *Phys. Rev. B* **92**, 241106(R) (2015).
- [39] E.-J. Kuo, B. Ware, P. Lunts, M. Hafezi, and C. D. White, Energy diffusion in weakly interacting chains with fermionic dissipation-assisted operator evolution, [arXiv:2311.17148](https://arxiv.org/abs/2311.17148).